ISOCAM: The Infrared Space Observatory Camera
Results of testing and calibrations

L. Vigroux, C. Cesarsky, O. Boulade, Y. Rio
Service d'Astrophysisque, CEN Saclay, F91191 Gif sur Yvette CEDEX, France

M. Perault, A. Abergel, F.X. Désert
Institut d'Astrophysique Spatiale, Campus d'Orsay, Bat. 120, F91405 Orsay CEDEX, France

D. Rouan, F. Lacombe
DESPA, Observatoire de Meudon, F92191 Meudon principal CEDEX, France

Abstract

ISOCAM, the ISO camera is designed to map selected regions of the sky in the spectral regions 2.5 to 17 microns. It will make images, within the 3 arcmin field of view of ISO with two 32 x 32 infrared array detectors, one for the short wavelength range, below 5 microns, the second for the long wavelength range, above 4.5 microns. Filter wheels and lens wheels allow to change the spectral resolution and the pixel field of view. Circular variable filters are also mounted on the filter wheel. The instrument is ready for delivery to ESA, after a thorough testing and calibration phase. Test has been conducted in a facility that simulate the ISO environnement. A particular care has been taken to ensure the appropriate level of IR background inside the calibration cryostat, to check the detectors in the actual IR flux range that they will experience in flight. This paper presents the results of this test and calibration campaign, with a particular emphasis on the optical performances and on the behaviour of the detectors. Photometric performances have been obatined for all the observing modes of ISOCAM. Some of these results, like stabilization of the detectors, have strong impacts on the observing strategy with ISOCAM.

1. Overview of ISOCAM

ISOCAM is one of the four focal plane instruments of the Infrared Space Observatory, ISO. It is a camera aiming to image the sky at various spatial resolutions in the wavelength range 2.5 to 17 μm. It is based on a double channels camera, a short wavelength channel, operating from 2.5 to 5 μm, and a long wavelength channel from 4 to 17 μm, both channels having a detector of 32 x 32 pixels, with 100 μm pixel pitch. Each channel includes a lens wheel carrying 4 lenses giving pixel field of view of 1.5, 3, 6, and 12 arcsec. The full coverage of the unvignetted 3 arcmin field of view of ISO is obtained for the 6 arcsec. lenses. Filter wheels are present in both channels. They hold 10 filters and low resolution Circular Variable Filters (CVF). A selection wheel allows to direct light through one or the other channel, or to illuminate the detectors with an internal calibration source. Polarimetry capabilities have been added by placing 3 polarizers on an entrance wheel.

ISOCAM was built by a consortium of European laboratories led by the Service d'Astrophysique of the Direction des Sciences de la Matiere of the Commissariat à l'Energie Atomique. In addition to the overall responsibility of the project, the SAp had the reponsibility of the LW detector and associated electronics. Meudon Observatory had the responsibility of the SW detector and electronics. The optical design and the procurement of the optical components was done by the Royal Observatory of Edinburgh, with the exception

0-8194-1182-5/93/$6.00

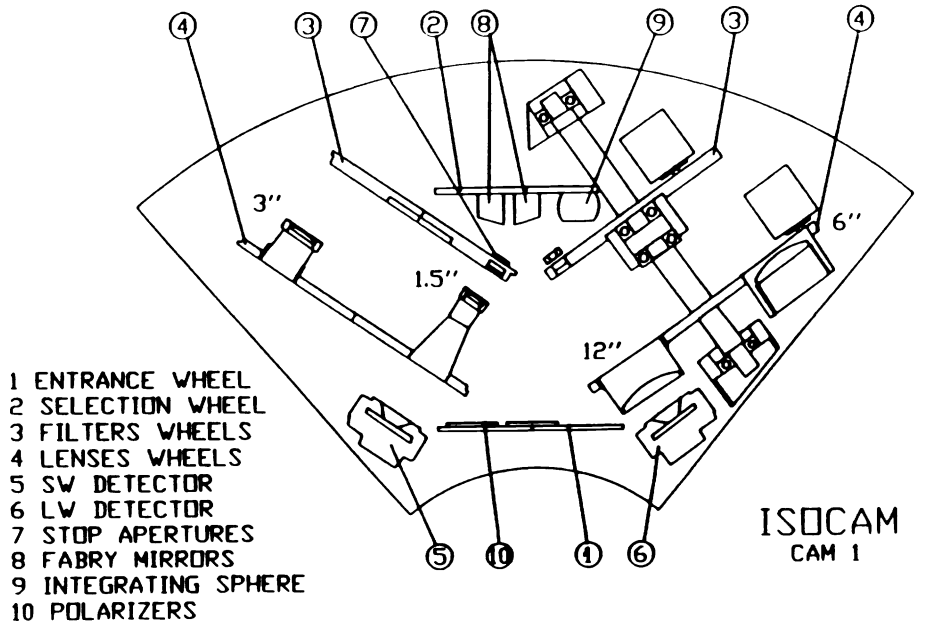

fig 1: ISOCAM layout

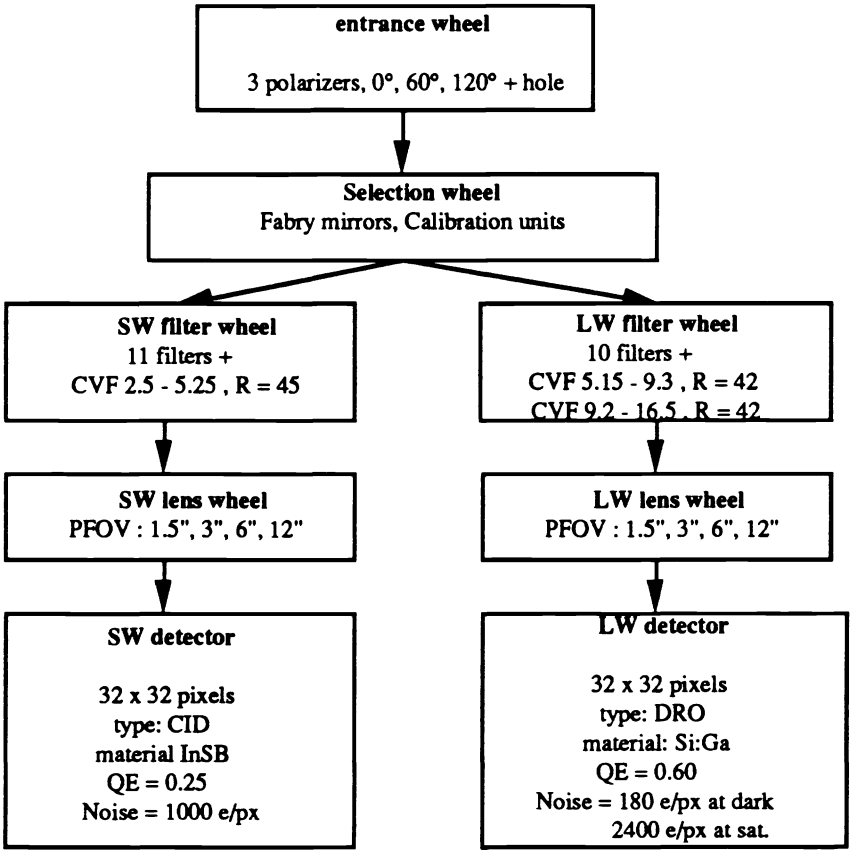

fig. 2: ISOCAM optical flow chart

of the filters which were done under the responsibility of the Stockholm Observatory. Italian laboratories from Bologna, TESRE and the Padova Observatory were responsible for ground support equipments. The optical bench has been subcontracted to Aerospatiale. The design of the camera started in 1986, and the flight model was ready to deliver to ESA after an extensive calibration at the end of 1992. This paper presents the instruments, the problems experienced during the development phases, and the performances achieved.

2. Cryomechanism

The ISOCAM mechanisms must whistand difficult constraints, cryogenic temperature, high reliability, low dissipation, and good positionning accuracy. Of course, they must be designed to survive the high level of vibrations during launch. To save developement time, we based the design of these mechanism around a supraconductor stepper motor developped by SAGEM which was already space qualified. The drawback of this solution was the small number of steps per turn, 24 and the high current required to drive the motor. A demultiplication gear train is required between the wheel and the motor to ensure the positionning of optical components. This is provided by a pinion on the motor axle driving the wheel through a gear on the egde of the wheel. The design of this gear must satisfy opposing constraints, large play to survive launch vibrations, smooth rotation to ensure reliability, and low frequency to minimize thermal dissipation. The first constraint was the driver for the design,and the gear has a play of 200 μm. Frequency in the range of 100 Hz was determined to minimized the shock due to the gear backlash, and to provide the specified lifetime of 100,000 revolutions. A motor drive current higher than normal is required for the first and last step of the rotation to communicate the initial kinetic energy to the wheel, and to avoid large number of shocks when the wheel stops. The motor pinion is built in VESPEL, a composite material made of polyimides and MoS2. Its elastic properties and its low friction coefficient at cold allow to avoid the deposit of solid lubrificant on the wheel gear, a solution which was experienced during the design phase of the cryomechanism, but which was found very fragile. With this design, the mechanisms have survived without noticeable degradations more than 200,000 cycles and qualification vibration levels at 4 K during the qualification phase. The drawback of this solution is the poor positionning accuracy, ± 100 μm, which is a source of problem, in particular for the reproducibility of the lens positionning.

The position encoding system relies on an absolute zero reference on the wheel and an incremental step counter. Both systems used magnetoresistor sensors. The incremental counter is built with 2 sensors, phased at 90°, sensing the passage of 24 teeth, 1 by motor step, situated on a wheel on the motor axle. The on board software verifies that the magnetoresistor counter is equal to the number of steps commanded to the motor. The zero reference is provided by a magnet on the wheel moving in front of a fix magnetoresistor. The only problem with this design was the large resistance variation with temperature found in some of the sensors. This was solved by a careful selection of the sensors selected from their properties at cold, after several thermal cycling.

3. The detectors

3.1 The LW detector

At the time of the ESA Call for Proposal, there was no detector available in Europe for the long wavelength channel. A specific development was undertaken at the Laboratoire d'Infrarouge, CEA-LETI in Grenoble. It is a photoconductor array in Gallium doped Silicon hybridized by Indium bumps to a direct voltage readout circuit. It has 32 x 32 pixels, 100 μm pitch with a thickness of 500 μm. The dopant concentration is 10^{16} cm^3, giving a resistivity of 10^{12} Ωcm. To obtain a 100% filling factor, the front surface is doped to ensure a good electrical conductivity and the photoconductor voltage is applied to an Aluminium frame on the side of the optical sensitive area. An 3 pixel wide external guard has been added around the 32 x 32 arrays to prevent field line distortion at the edges. On the back surface, a reflector electrode is placed between the indium

bump, with 2 effects,: first to increase the reflection coefficient of the back surface, and therefore the overall quantum efficiency, and to provide a good electrical separation between adjacent pixels. Despite the absence

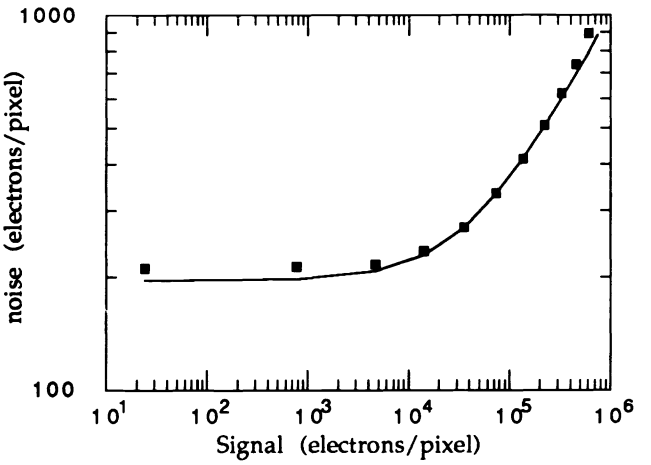

fig 3: noise characteristic of the LW detector. This curve corresponds to the high freqency term of the noise. The points are the results of measures, and the curve is a model assuming a constant readout noise of 200 e^-px^{-1} and photon shot noise

of a front grid, this detector has a very low optical crosstalk. For the fastest lens of the camera, the 12" lens which has a numerical aperture of f/1, the optical crosstalk remains below 1.5%.

The readout circuit has one integration capacitance of 0.12 pF and a MOS follower with a gain of 0.8. A 3 among 7 coding allows to adress pixels on the 32 outputs lines. We use a double sampling readout scheme, first reset the output capacitance and measure this reset level, then integrate and measure the level at the end of the integration. The onboard electronics provides programmable bias voltages for the photoconductor and for the readout circuits, as well as programmable integration time. The analog electronics feeds a 12 bits A/D converter, common to both channels. Gain of the chain can be selected between 1, 2 or 4 to allow a good sampling of the noise in low flux conditions, and to take advantage of the whole dynamic of the detector. In the lowest gain, 1 AD unit is ≈ 240 electrons. Typical integration time in flight will be between 0.2 and 20 seconds. The noise characteristic of this system presents several components, a high frequency term which is well approximated by a constant readout noise of ≈ 200 e^-px^{-1} and photon shot noise, and a low frequency noise which becomes important after ≈ 50 readouts. At high level, > 510^5 e^-px^{-1}, an amplifier noise becomes preponderant and limits the Signal to Noise ratio to ≤ 500 in a single image.

Stabilization after changes of flux or integration time is the main problem encountered with this detector. We found that the stabilization time gets worse when we increase the photoconductor voltage. We used a 25 V polarization as the optimum trade off between detector responsivity and stabilization overhead. With this voltage, the responsivity at 15 μm is 10^{14} V/W for 1 sec integration time, which corresponds to a photogain, quantum efficiency product, $\eta g \approx 1$. Stabilization remains a problem in two cases, illuminating the detector previously at dark, or after a saturating flux. The first problem can be overcomed by keeping awlays light on the detector and sorting the sequences of observations by decreasing fluxes. After a saturation, the detector keeps memory of the illuminating scene for period as long as half an hour. The only way we found to avoid polluting new observations with the memory image is to saturate the whole array with a uniform illumination. With a flash duration of a couple of readouts, the detector looses memory of the previous scene, and can be used to image the new field. The drawback of this method is that after the flash, the overall responsivity of the detector will be below the average value for about 10 minutes. This effect decreases the

absolute photometric accuracy, but allows to keep a reasonnable relative photometric accuracy inside an image. This procedure will be used only in real time commanding, when the quick look analysis of the observations has shown that there were saturated pixels in the images.

Flat fielding accuracy can be as good as 5 10^{-3} when the detector is stabilized. Better accuracy may be achieved by using a non linear flat fielding algorithm which is currently under investigation. The flat field of the detector was found to be very stable all along the calibration; this allow the use of a flat field library, instead of loosing observing time by making a flat field calibration with the internal calibration device linked with each new observation. However, a limitation comes from the differential stabilization times between pixels in the array. It would be prohibitive in flight to wait for a full stabilization of the detector, and we must start the observations in still unstable configurations. Usually, stabilization is quantified by comparing the mean pixel signal to the stabilized value. In our case, it is better to determine the stabilization by measuring the pattern noise on flat fielded images. The differential stabilization generates a pattern accross the images which increases the spatial noise. Low level effects can be observed on several tens of minutes after a flux step. A good way to remove these small effects is to use a beam switching procedure, switching the pointing from the source to an adjacent background, as done on ground based telescope. This can be done using the raster pointing mode of ISO. The switching period must be of the order of 20 readouts to ensure a coherent flat field between the observations on the source and on the background, and to minimize the low frequency noise.

Another limitation of the sensitivity of the LW detector is due to the responsivity variations and glitches due to the impact of charged particles. These particles comes from trapped particles in the Van Allen belt and from galactic cosmic rays. Extensive radiation tests were performed with γ rays sources, protons and heavy ions accelerator beams. Two main regimes can be found. In the Van Allen belt, the ionizing radiation is very high and induces a responsivity increase which relaxes in a few hours. We found that this effect is minimized if we keep the photoconductor polarized and exposed to a high infrared flux. Since the experiment is switch off in the Van Allen belt, we design a specific power suply using the Keep Alive line provided by the satellite to keep some voltages on the photoconductor, and we leave the camera open during the perigee passage. With this procedure, our test results show that the responsivity variation must remain below 5% in the good part of the orbit. Outside the belts, the expected impact rates are 1 proton/second, and 1 heavy ion/15 minutes on the array. Each particle will generate a glitch followed by a decrease of responsivity. Proton and heavy ions glitches can be easilliy removed from the observation by filtering technics. The worse problem is the responsivity variation after the glitch, especially for heavy ions. Detailed modelling of these effects are under investigations, but they will have to be tuned up with real flight data.

3.2 The SW detector

For the short wavelength channel, the basic device is a 32 x 32 pixels CID InSb array manufactured by the Société Anonyme de Télécommunications. This detector was already qualified and presented the advantages of a low operating temperature and a large radiation tolerance compatible with the ISO mission. Upgrades of the existing devices have been made along several tracks: increase of the pixel pitch up to 100 μm, increment of the surface filling factor to 89%, and a new design of the supporting ceramic to reduce electrical cross talk. A control and readout hybrid electronics was designed to work at 4K closeby to the chip. The detector and its cold electronic are housed behind an aluminium cover which provides a shield for radiation and stray light. Measurements of the pixel charges can be done by sensing the voltages of the 32 output lines and sequentially injecting the pixel charges in the substrate through column voltage clocks. The analog chain used an adaptive filter followed by high gain preamplifiers. The output signal is nevertheless very small, a few μV, and the lines are very easily affected by pick up noise. To calibrate the pick up, 2 blind lines were added in the detectors and the electronic chain. These lines are used as a reference for the correlated pick up noise. A correlation matrix can be determined between the pixels on the reference lines and the actual pixels, and used to remove the correlated noise. This procedures is very efficient. For exemple, during EMC test, the raw noise

increases by a factor of 50 at certain radiated frequencies, and the decorrelation using the references lines allowed to get the noise level back to the normal values. After the subtraction of the correlated noise, the remaining noise can be very well modelized by a constant readout noise and photon shot noise.

As for the LW detector, the stabilization times are a problem. The stabilization times appear to be a function of together the initial and final IR fluxes. They are of a few ($\approx$ 10) readouts for large flux steps but become prohibitively long for small flux step starting from dark. Unfortunately, in the SW channel wavelength range, the IR background is very low, a few ADU/sec. at maximum, and the situation which will be encountered during all the observations of faint sources is indeed the worst case. The sensitivity is limited by the stabilization time, and not by the noise. To overcome this problem, we tried several observing procedures. The best results is obtained by a flash of the detector done with our internal calibration device at the beginning of the observations. The astronomical sources are observed during the slow decay of the detector after the flash. In a second step, we reproduce the same flash and slow decay, closing the entrance wheel of the camera. Subtraction of this reference decay allows to reveal the faint sources. The flashing procedure allows to reproduce the flash with a few percent accuracy. With this procedure we have been able to detect sources in the mJy range, in 20 min. observing time, while a normal observations would have required several hours due to the slow stabilization. In this observing mode, we can recover the noise limited sensitivity which is a few tenth of mJy in 1 hour at 3 σ level.

4. The internal Calibration Device

The internal calibration device was designed to provide an internal flat field source, and a rough photometric calibration reference. Calibration of the SW channel required sources near 350 K which are difficult to fit in the low thermal dissipation allocation of ISO, less than 10 mW as a mean. The solution is small resistor, 0.6 mm^2, mounted on a thin kapton film. The low thermal conductivity of the kapton prevents heat losses towards the ISOCAM base plate and ensure that almost all the energy is radiated. The peak dissipation remains below 20 mW. The mechanical support of this emitter was designed to compensate the dilatation of the kapton film when the resistor is heated, to keep it always at the same position. This emitter feeds an integrating sphere which is supported on the selection wheel. In calibration mode, the integrating sphere is at the location of the field mirror. The lack of room in the selection wheel environment restricts the diameter of the sphere, and there is as few as one or two reflections between input and output rays. A high scattering surface was achieved by machining the sphere in a single block of Al, with an electrochemical erosion of the internal surface. The output uniformity is better than 1% in the unvignetted circular 3 arcmin. field of view of ISOCAM. Two spheres are included in the system, one for each channel, with entrance holes adapted to the flux required for each detector. The temperature of the emitter can vary in the range 120 K to 350 K, and is controlled by a 12 bits programmable DC current generator.

This design has two limitations. On the optical side, the calibration beam etendue is defined only by the aperture stop at the filter location. It is different from the ISO telescope f/15 beam. Nevertheless, a good flat field can be obtained with the 1.5 arcsec. and the 3 arcsec lenses. The second comes from the addition of some low level emission of the kapton support which is heated by conduction. This effect can be seen at long wavelength, where there are some kapton bands present in the spectrum of our calibration device. This would preclude the use of this system as an absolute flux calibration reference. However, it is of little importance for ISOCAM, since we will use it only as a relative reference standard. This device has been used all along the integration and calibration phases of the flight model, on a 1 year and half time scale. During this period, a routine monitoring of the instrument has shown that the reproducibility of the calibration system is better than 10%, in all the configurations of ISOCAM, channel, filter and lenses.

5. Optical performances of ISOCAM

The calibration of the ISOCAM performances was performed at the Institut d'Astrophysique Spatiale in Orsay. It was done in a dedicated facility which simulates the flight environment. The most difficult achievement of this facility was to provide the low infrared background expected during the flight. In flight, the background, in the ISOCAM wavelength range, is only due to the zodiacal light. This is a factor > 10^7 less than the background obtained with hot (300 K) window in front of the camera. The background specification on the whole CAM wavelength range corresponds to a maximum temperature of 27 K of all of the elements within the direct field of view of the detectors. Such a low background can only be achieved by considering a closed cryostat. All the optical components, ISO telescope simulator and the calibration sources are supported on a single 1 m diameter optical table, which is the cover of a liquid helium tank. Light tightness was ensure by a cold inner thermal screen at 20 K all around the optical table and a careful baffling of all the service holes, filling and evacuation pipes, harness,...The background measured during the first test sequence was nevertheless too high, and an additional cover, black painted, was put above the optical elements and the camera, on the table. A background level less than 0.1 of the zodiacal background has been achieved

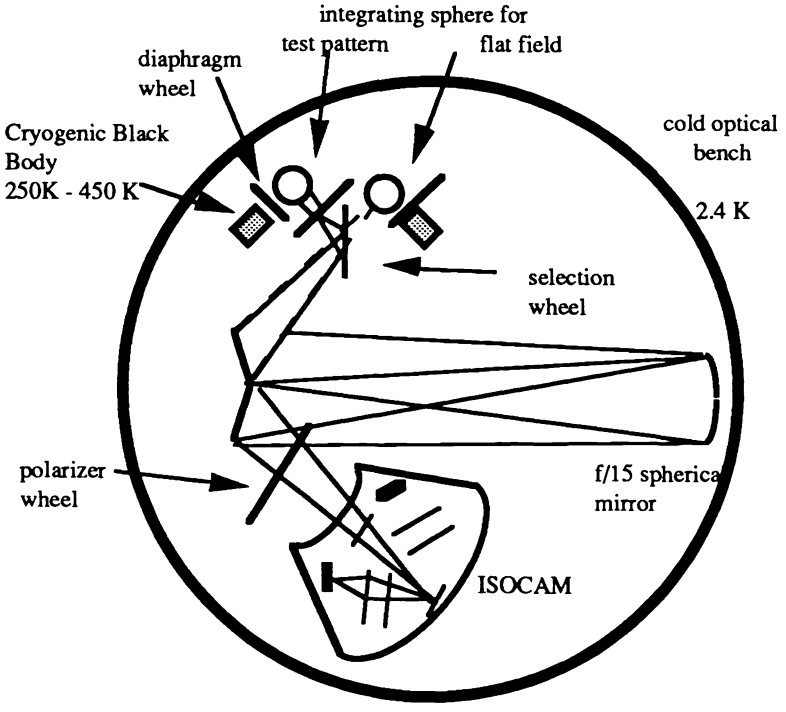

figure 4: layout of the ISOCAM calibration facility

An other strong requirement was to simulate the actual observation with faint sources superposed on the Zodiacal background. The telescope simulator is fed by 2 different sources. A flat field source provides a flat illumination over the ISO field of 3 arc minutes, and a point source is used to simulate star like objects. A

commutation wheel allows to send either the point source or the flat field on the camera. The wheel also houses a semi reflecting germanium window which allows the mixing of the light from the 2 sources. These sources are based on a cryogenic black body with temperature from 200 K to 450 K, which illuminate integrating spheres through a diaphragm wheel which holds several calibrated holes and neutral densities. The point source is provided by a 80 μm hole in a nickel plate. This plate can be moved with a resolution of 16 μm in 3 axes, along the optical axis for focalisation, and in the perpendicular plane to explore the ISOCAM field of view. In addition to the cryogenic source, the flat field sphere can be illuminated by a monochromatic beam coming from a hot black body and a monochromator situated outside the cryostat to perform spectral measurements such as filter or CVF transmission. All the motions were controlled by magneto resistor sensors. They use customized cryogenic stepper motors developed by F. Sirou (Laboratoire de Météorologie Dynamique) from commercialized stepper motors. All the simulator is remotely controled by a Vax station linked through a network to the Vax station used as test equipment for ISOCAM. This configuration permits fully automatized test sequences, interleaving CAM and simulator commands.

After the delivery of the optical bench from Aérospatiale, the flight detectors are set up inside CAM at their theoretical location derived from the Aérospatiale focalisation measurements. Tests of focus positions must be performed with these detectors for the 4 magnification lenses on each channel. In focalisation procedure, the focus is achieved by the motion of the point source along the optical axis. The accuracy of the measurements is 1.0 mm, both for the simulator focus and the CAM focus positions. This is mainly due to the astigmatism of the off-axis mirror, but is is still smaller than the ± 2 mm positioning accuracy ensured during the CAM integration on the ISO telescope which has been taken into account in the error budget for the image quality. The best focus, assumed to be the middle of the 2 sagital foci, is within 1 mm of the simulator focus for all the lenses of ISOCAM.

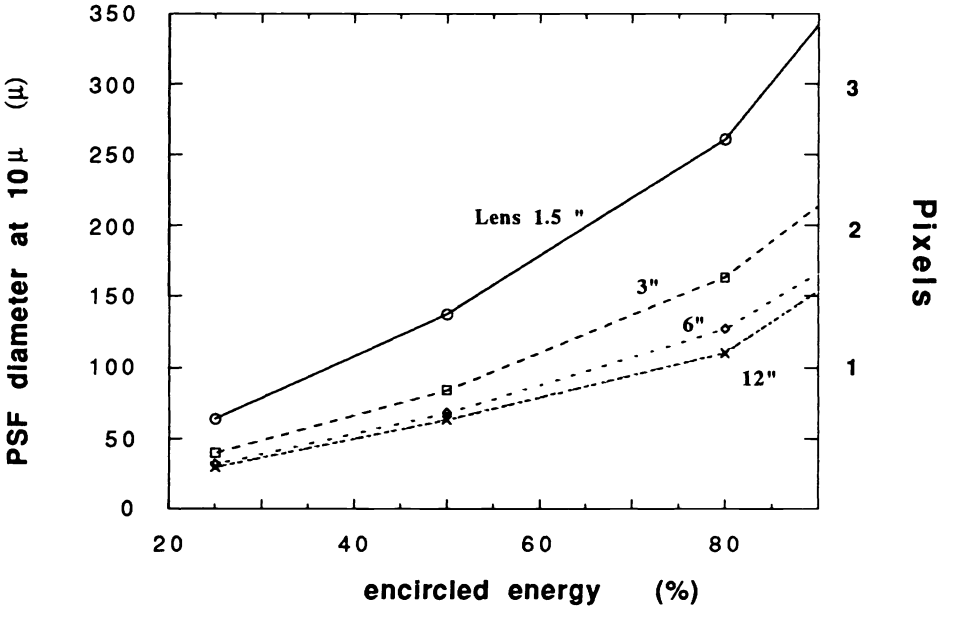

Figure 5: ISOCAM PSF at 10 μm for the 4 Pixel Fields of View

The point spread function is a convolution of the detector pixel sampling, and of the optical PSF. PSF measurements were performed by a scan of the point source along the y and z axis of the camera, corresponding

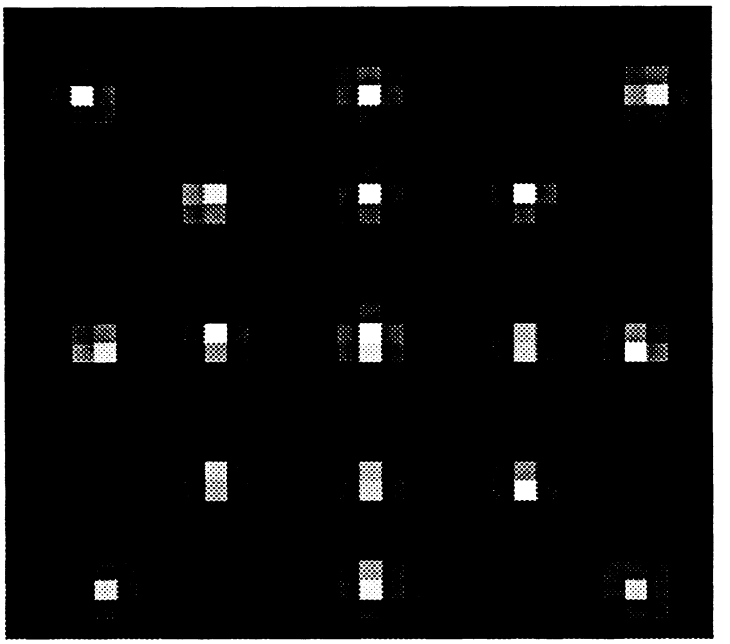

fig 6 : images of a point source obtained with the 6 arcsec. pixel field of view lens, at various location in the 3 arcmin. field of view of ISOCAM

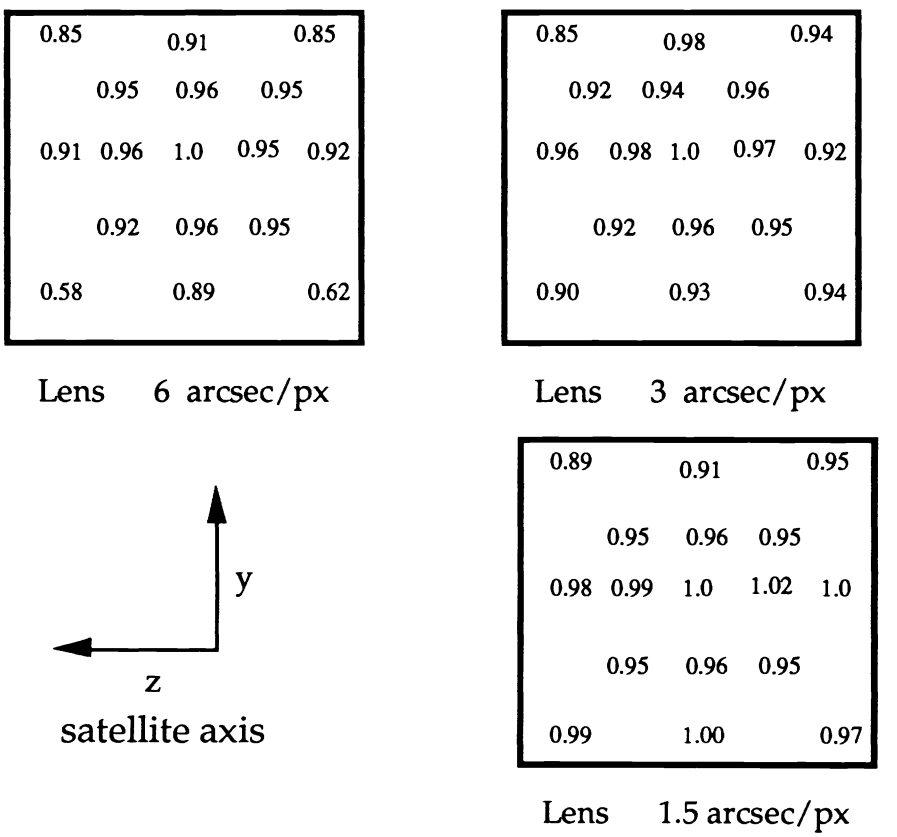

figure 7: vignetting determined with point sources for the lenses 1.5, 3 and 6 arcsec.

to the columns and the rows of the detectors, with a step of 1/4 to 1/8 of the pixel pitch over 5 pixels. The PSF were calculated by recentering and coadding individual images. The dynamic achieved is greater than 3000 for all the lenses. The resulting PSF obtained are almost identical to the theoretical predictions obtained by the convolution of single lens PSFs measured at ROE by a 100 μm width square function. For lenses 12 and 6 arcsec., the ISOCAM resolution is limited by the pixel sampling. A good sampling of the PSF is provided only by the 1.5 arcsec. lens.

Vignetting was measured by moving the point source at 17 different positions on the detectors for each lenses. Figure 7 shows the results obtained for the 1.5, 3 and 6 arcsec. lenses on the LW channel. The accuracy of the measurement is 2%, and was determined by carrying out repetitive measurements of the intensity at the central position throughout the duration of the test. No significant vignetting is found for the 1.5 and the 3 arcsec. lens, while transmission losses of 20% were found on the corner of the detectors with the 6 arcsec. lens. This is due to the original design of the camera which was dimensioned for a circular 3 arcmin. field of view corresponding to the unvignetted field of view provided by ISO. In the development phase, the field of view was increased to a square 3 arcmin. field to take advantage of the square shape of the detector, but since the corners were already in the vignetted field of the telescope, we did not increase the size of the 6 arcsec. lens to accommodate this larger field of view. Vignetting in the specified circular 3 arcmin. field remains lower than 5%.

Stray light analysis was achieved in several ways. One method moved the point source in a field of 9 arc min. to look for unexpected reflections, outside the normal field of the camera. Another method used the flat field source with two diaphragms providing a 4 arcmin, and a 9 arcmin. fields. It has been used to check for integrated stray light problem. The tests undertaken highlighted that the main origin of stray light was caused by reflections occuring in the neighborhood of the detectors.

This is demonstrated by the 3 arcsec. lens which provides a detector field of view of the detector of 1.5 arcmin. The light incident on the field mirror, outside the detector field, but nevertheless in the camera field of 3 arcmin., illuminates the side of the detectors, where are the connecting gold strips. A multiple reflection

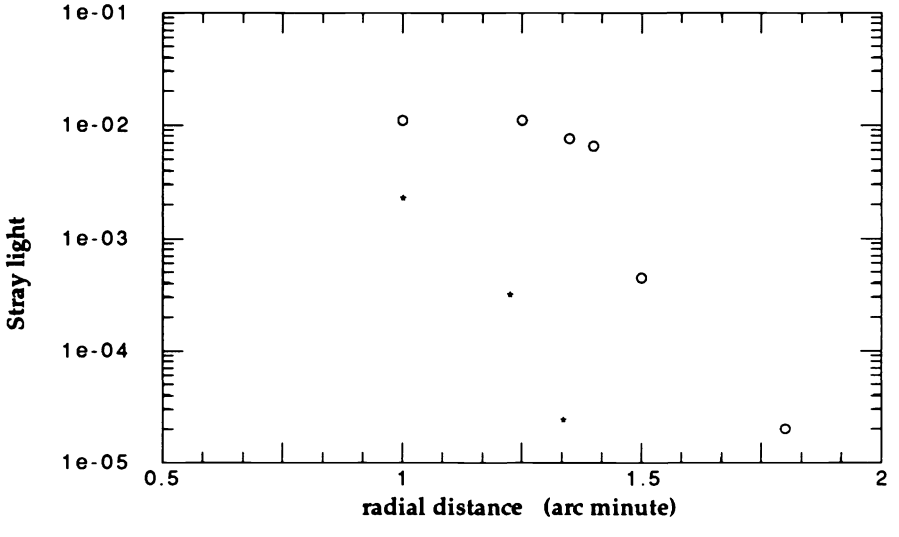

Figure 8: stray light profile obtained with the 3 arcsec. lens and the 2 field mirrors, circles: large Fabry mirror, stars: small Fabry mirror

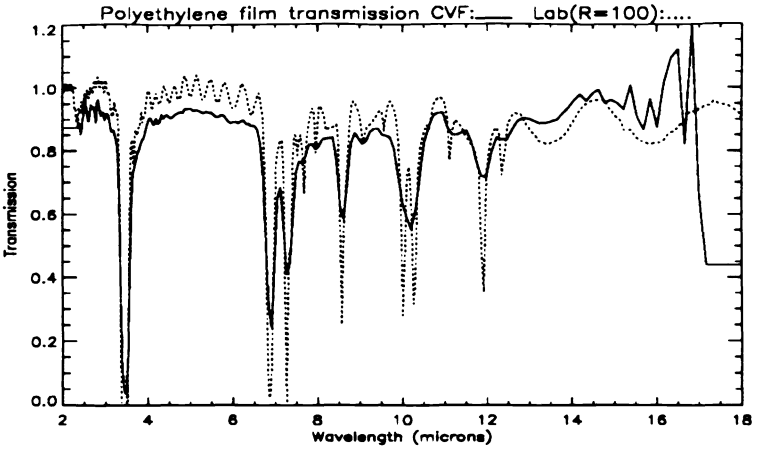

fig 9: spectrum of a polyethylene film obtained with the ISOCAM CVF.

system with the filters creates a strong ghost image. With the 6 arcmin. lens, the ghost images are due to reflection on the detector itself. By tilting the filters by an angle of 5° in their mounts most of the stray light was eliminated. However, it was not possible to tilt the Circular Variable Filters, and we added in the system a field mirror adapted to the 1.5 arcmin. field of view for the CVFs. Figure 5 shows the stray light rates obtained with the 3 arcsec. lens on the LW channel for the normal and the small field mirror. The larger rate with the large field mirror is mainly due to the normal wings of the PSF. With these late modifications of the optical bench, the stray light performances of the camera, while not outstanding, are within the specifications and will preserve all the foreseen scientific uses.

With the external monochromator, the calibration facility was used to measure the filter transmission, the detector relative spectral response, and to obtain a full characterization of the CVFs. Inside ISOCAM, the whole wavelength coverage is provided by 3 CVF segments, 1 on the SW channel, from 2.5 to 5 μm, and 2 on the LW channel from 5 to 9 and 9 to 16 μm, with some overlap regions at 9 μm. For the CVF, we have determined the position angle - wavelength law, and the spectral resolution. Basically, they have a linear wavelength transformation law. The CVFs alone have an almost constant resolution, R ≈ 45 all over the wavelength range. In ISOCAM, the pupil diameter at the CVF level is 2.4 mm. Therefore, the resolution is the convolution of the intrinsic CVF resolution broadened by the difference of central wavelength across the pupil image. As a result, the resolution decreases with wavelength on each of the 3 CVF segments. It starts from 40 in the short wavelength region and ends to 45 at long wavelength. The resolution of the CVFs were measured in two ways, scanning a monochromatic line with the CVF, or scanning the monochromator keeping the CVF at a fix position. As a verification of the calibration we took the spectra of the monochromator black body seen through transparent plastic films in polyethylen or polystiren of known spectral transmissions. Fig 9 show the comparison of the CAM CVF spectra and the transmission curve of the polyethylen film measured on an infrared spectrograph with a resolution of 100.

Our calibration provided us with the characteristic of all the individual components of the instruments, filters, lenses, detectors. With this information, it is possible to built a photometric model of the camera which can be used to predict the performances in flight to prepare the scientific observations. As a test, we compare the results of this model with the actual measurements in the calibration facility. Fig 10 shows the results of this compararison for 3 filters. each point corresponds to an individual measurement obtained with an independant setting of ISOCAM, and the calibration simulator. The calibration black body temperatures used span the whole range available, from 250 K to 450 K. The mean predictions of the photometric model to

measurements ratios are 1.09 at 5 μm, 1.15 at 9 μm and 0.93 at 15 μm. As a mean, our photometric model provides an absolute accuracy of 10%.

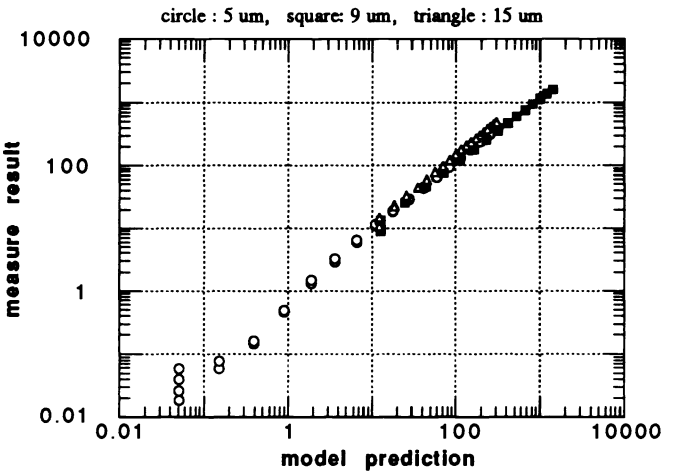

fig 10 : comparison between the photometric model prediction and actual measurements made with ISOCAM in the calibration facility

6. Conclusions

ISOCAM is the first of a new generation of complex infrared instruments, using infrared arrays, to be used on a cryogenic spacecraft. The original scientific specifications were challenging in several domains, detectors performances, cryomechanics, and optical design with regards to the severe constraints imposed by ISO. Most of the difficulties have been overcome during definition studies and during the testing of the qualification model. Minor modifications to improve stray light has been brought after the fisrt optical test of the flight model. After the calibration of the flight model, we know that ISOCAM performances are within the expected range to carry out the scientific programs for which it has been designed. ISOCAM will provide images with spatial resolution of ≈ 3 to 6 arcsec, spectral resolution of ≈ 5 to 45 of sources as faint as a tenth of mJy. Compared to IRAS at 10 μm, It correspond to a gain of more than 500 for point source detection, and a gain of 10 in spatial resolution for extended objects. Compared to the present new generation of ground based cameras at 10 μm, the ISOCAM sensitivity on point source is 100 times better, but of course the spatial resolution of ISOCAM is poorer than ground based images for bright objects.